JOURNAL OF THEORETICAL
AND APPLIED MECHANICS
56, 2, pp. 497-510, Warsaw 2018
DOI: 10.15632/jtam-pl.56.2.497

EFFECT OF CYCLIC HARDENING ON STRESS RELAXATION IN SUS316HTP UNDER CREEP-FATIGUE LOADING AT 700°C: EXPERIMENTS AND SIMULATIONS

Nobutada Ohno

Nagoya Industrial Science Research Institute, Nagoya, Japan

e-mail: nobuohno@nagoya-u.jp; nobuohno@nifty.com

Tatsuya Sasaki

Department of Computational Science and Engineering, Nagoya University, Nagoya, Japan

e-mail: t.sasaki@mml.mech.nagoya-u.ac.jp

Takehiro Shimada, Kenji Tokuda, Kimiaki Yoshida

IHI Corporation, Yokohama, Japan

e-mail: takehiro_shimada@ihi.co.jp; kenji_tokuda@ihi.co.jp; kimiaki_yoshida@ihi.co.jp

Dai Okumura

Department of Mechanical Engineering, Osaka University, Osaka, Japan

e-mail: okumura@mech.eng.osaka-u.ac.jp

Cyclic hardening and stress relaxation experiments of SUS316HTP were performed under creep-fatigue loading with tensile strain holding at 700°C. Experiments revealed that under strain holding, the slow stress-relaxation stage satisfying Norton's law with slight cyclic hardening followed a rapid stress-relaxation stage that was noticeably affected by cyclic hardening. This suggests that in the slow stress-relaxation stage, inelastic deformation mechanisms different from that of viscoplasticity occurred. Experiments were simulated using a cyclic viscoplastic-creep model in which the inelastic strain-rate was decomposed into viscoplastic and creep components that were affected differently by cyclic hardening. The simulation accurately reproduced the experiments.

Keywords: creep-fatigue loading, cyclic hardening, stress relaxation, SUS316, constitutive model

1. Introduction

Creep-fatigue tests with tensile and/or compressive strain holding at high temperatures have been performed to investigate the effect of creep damage on the fatigue lives of materials. For polycrystalline metals, creep damage under creep-fatigue loading is caused by grain boundary cavitation that develops with the accumulation of creep strain under strain holding (e.g., Hales, 1980; Priest and Ellison, 1981; Nam, 2002), and has been macroscopically evaluated in terms of the changes in stress and creep strain under strain holding (e.g., Inoue *et al.*, 1989; Takahashi *et al.*, 2008; Yan *et al.*, 2015). To numerically evaluate creep damage in structural components, it is necessary to use a constitutive model that can accurately simulate the stress-strain behavior under cyclic loading with strain holding.

The ductility exhaustion method proposed by Priest and Ellison (1981) and Hales (1983) is a well-known method to evaluate creep damage under creep-fatigue loading (Ainsworth, 2006; Yan *et al.*, 2015). This method assumes that creep damage develops with the accumulation of creep or inelastic strain under strain holding. Priest and Ellison (1981) proposed that creep damage develops when the inelastic strain-rate under strain holding is smaller than the transition rate

below which the diffusion creep and grain boundary sliding become important, whereas Hales (1983) considered that the development of creep damage depends on the variations in inelastic strain in three periods under strain holding. Takahashi (1998) and Takahashi *et al.* (2008) adopted the Priest and Ellison (1981) model and decomposed the inelastic strain-rate under strain holding into viscoplastic and creep components occurring at high and low inelastic-strain rates, respectively, and assumed that only the creep component contributes to the development of creep damage. They thus accurately predicted the creep-fatigue lives of 316 stainless steel at 550°C and 600°C.

The decomposition of inelastic strain-rate is physically valid in the presence of dislocation viscoplasticity at high inelastic strain-rates and diffusion creep at low inelastic strain-rates. In the constitutive modeling of cyclic plasticity, however, the decomposition of inelastic strain into viscoplastic and creep strains has been regarded as a conventional assumption. The work has been focused on the development of unified constitutive models, in which both viscoplasticity and creep are considered to be caused by dislocation movements (Miller, 1976; Krausz and Krausz, 1996; Chaboche, 2008). It is, therefore, worthwhile to investigate the stress relaxation behavior in creep-fatigue tests to examine the appropriateness of the inelastic strain-rate decomposition. This point of view was not taken by Nouailhas (1989) for using a unified model to simulate the creep-fatigue tests of 316 stainless steel at 600°C performed by Goodall *et al.* (1981).

In this study, the stress relaxation behavior under tensile strain holding was measured in creep-fatigue tests of SUS316HTP at 700°C to examine the decomposition of inelastic strain--rate. It was assumed that the increase in dislocation density, which occurs in grains and is observed as cyclic hardening, affected viscoplasticity significantly more than diffusion creep and grain boundary sliding. It was thus suggested that inelastic deformation mechanisms other than viscoplasticity started to operate shortly after the onset of strain holding, and consequently that the inelastic strain-rate consisted of viscoplastic and creep components under strain holding in the creep-fatigue tests. The experiments were then simulated using a cyclic viscoplastic-creep model in which cyclic hardening was assumed to have different effects on the viscoplastic and creep strain-rates.

Throughout this paper, a superposed dot indicates differentiation with respect to time t, a colon represents the inner product between tensors (e.g., $\boldsymbol{\sigma} : \boldsymbol{\varepsilon} = \sigma_{ij}\varepsilon_{ij}$ and $\mathbf{D} : \boldsymbol{\varepsilon} = D_{ijkl}\varepsilon_{kl}$), $\|\cdot\|$ denotes the Euclidean norm of second rank tensors (e.g., $\|\boldsymbol{\sigma}\| = (\boldsymbol{\sigma} : \boldsymbol{\sigma})^{1/2}$), and $\langle\cdot\rangle$ indicates the Macaulay brackets (i.e., $\langle x\rangle = x$ if $x > 0$ and $\langle x\rangle = 0$ if $x \leqslant 0$).

2. Experiments

2.1. Material tested and cyclic loading conditions

Uniaxial creep-fatigue tests with tensile strain holding were performed at 700°C using an electric-hydraulic servo-type material testing machine MTS810. The material tested was SUS316HTP (a 316 stainless steel), which had the chemical composition and mechanical properties at room temperature given in Tables 1 and 2. Solid bar specimens with the shape illustrated in Fig. 1 were used. The tests performed are listed in Table 3. Hereafter, $\Delta\varepsilon$, $\dot{\varepsilon}$, and t_h indicate the strain range, strain-rate, and strain hold time, respectively, in the creep-fatigue tests.

Table 1. Chemical composition of SUS316HTP by mass percent

C	Si	Mn	P	S	Ni	Cr	Mo
0.07	0.28	1.75	0.27	0.0	11.2	16.6	2.12

Table 2. Mechanical properties at room temperature

0.2% proof stress [MPa]	Tensile strength [MPa]	Tensile rupture strain [%]
267	553	68

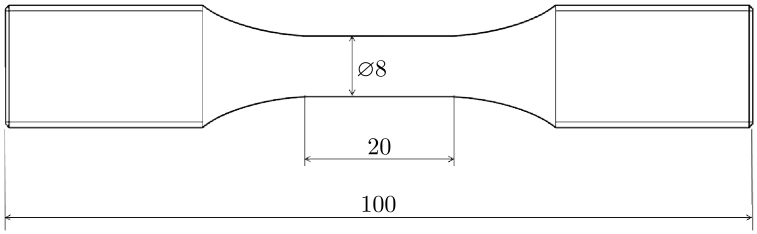

Fig. 1. Shape of the experimental specimens; dimensions in mm

Table 3. Tests performed

Strain rate [1/s]	Strain range [–]	Tensile strain hold time [min]
10^{-3}	0.010	0, 10, 60
10^{-3}	0.007	0, 10, 60
10^{-3}	0.004	0
10^{-4}	0.010	0

2.2. Effect of cyclic hardening on stress relaxation

The effect of cyclic hardening on the stress relaxation behavior under strain holding was investigated using the experimental data obtained in the creep-fatigue tests with $t_h = 60\,\text{min}$.

Under stain holding, we have

$$\dot{\varepsilon} = \dot{\varepsilon}^e + \dot{\varepsilon}^{in} = 0 \tag{2.1}$$

where $\dot{\varepsilon}^e$ and $\dot{\varepsilon}^{in}$ are the elastic and inelastic parts of $\dot{\varepsilon}$, respectively. Assuming isothermal Hooke's law for $\dot{\varepsilon}^e$ in Eq. (2.1) gives

$$\dot{\varepsilon}^{in} = -\frac{\dot{\sigma}}{E} \tag{2.2}$$

Here, σ and E indicate the uniaxial tensile stress and Young's modulus, respectively. Using a difference approximation for $\dot{\sigma}$ in the above equation, $\dot{\varepsilon}^{in}$ at time t is represented as

$$\dot{\varepsilon}^{in}(t) = -\frac{\sigma(t_{i+1}) - \sigma(t_i)}{(t_{i+1} - t_i)E} \tag{2.3}$$

where t_i and t_{i+1} are times slightly before and after t, respectively.

Applying Eq. (2.3) to the experimental data at $\dot{\varepsilon} = 10^{-3}\,\text{s}^{-1}$ with $t_h = 60\,\text{min}$ at $\Delta\varepsilon = 0.007$ and 0.01 provided the relationships between $\log\sigma(t)$ and $\log\dot{\varepsilon}^{in}(t)$ under strain holding (Figs. 2a and 2b). Stress increased with the increasing number of cycles N, especially in the stage just after the onset of strain holding. This is the phenomenon known as cyclic hardening. The relationship became linear to satisfy Norton's law shortly after the onset of tensile strain holding. Hereafter, the stage of stress relaxation satisfying Norton's law is referred to as the Norton stage, and is distinguished from the transient stage in which stress rapidly relaxes just after the onset of strain holding. Figure 2 shows that the Norton stage had much less cyclic hardening than the transient stage.

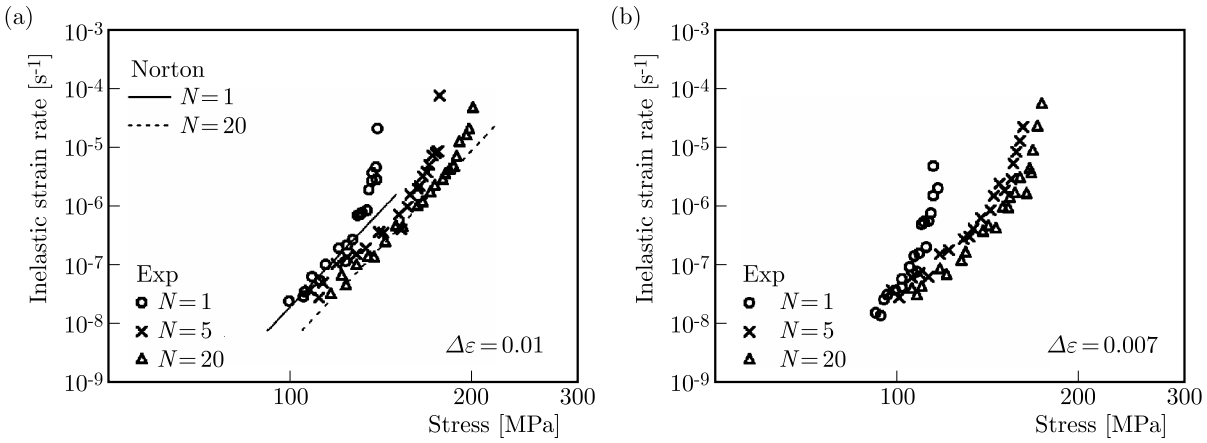

Fig. 2. Relationship between $\dot{\varepsilon}^{in}$ and σ under tensile strain holding in the creep-fatigue tests at $\dot{\varepsilon} = 10^{-3}\,\mathrm{s}^{-1}$ with $t_h = 60\,\mathrm{min}$ at: (a) $\Delta\varepsilon = 0.01$ and (b) $\Delta\varepsilon = 0.007$

To discuss the effect of cyclic hardening on the stress relaxation in more detail, the tensile peak stress σ_{+peak} and a representative stress in the Norton stage, $\sigma_{10\mathrm{E}-7}$, are plotted against N in Fig. 3. Here, $\sigma_{10\mathrm{E}-7}$ denotes the stress at which $\dot{\varepsilon}^{in}$ became equal to $10^{-7}\,\mathrm{s}^{-1}$ under strain holding. As seen in the figure, $\sigma_{10\mathrm{E}-7}$ increased slightly with N compared to σ_{+peak}, which increased noticeably from $N = 1$ to $N \approx 20$. This confirms that the Norton stage had much less cyclic hardening than the transient stage. It is physically valid to assume that cyclic hardening is primarily caused by an increase in dislocation density, which occurs in grains and is responsible for viscoplasticity. It is thus suggested that the Norton stage is rate-controlled by inelastic deformation mechanisms such as diffusion creep and grain boundary sliding, which are different from viscoplasticity. Therefore, to simulate the creep-fatigue tests performed in this study, the inelastic strain-rate under strain holding should be decomposed into a viscoplastic component responsible for the transient stage and a creep component responsible for the Norton stage.

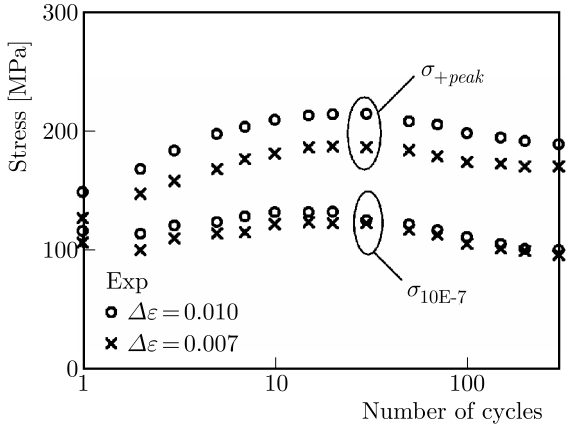

Fig. 3. Variations in σ_{+peak} and $\sigma_{10\mathrm{E}-7}$ with N and $\Delta\varepsilon$ in the creep-fatigue tests at $\dot{\varepsilon} = 10^{-3}\,\mathrm{s}^{-1}$ with $t_h = 60\,\mathrm{min}$

3. Constitutive model

Because the inelastic-strain rate under strain holding is decomposed into viscoplastic and creep components (Section 2.2), it is assumed that the strain-rate $\dot{\boldsymbol{\varepsilon}}$ is decomposed into an elastic component $\dot{\boldsymbol{\varepsilon}}^e$ obeying Hooke's law, a viscoplastic component $\dot{\boldsymbol{\varepsilon}}^p$ associated with combined

isotropic-kinematic hardening, and a creep component $\dot{\boldsymbol{\varepsilon}}^c$ satisfying Norton's law[1]

$$\dot{\boldsymbol{\varepsilon}} = \dot{\boldsymbol{\varepsilon}}^e + \dot{\boldsymbol{\varepsilon}}^p + \dot{\boldsymbol{\varepsilon}}^c \qquad \boldsymbol{\sigma} = \mathbf{D}^e : \boldsymbol{\varepsilon}^e \tag{3.1}$$

and

$$\dot{\boldsymbol{\varepsilon}}^p = \frac{3}{2}\dot{\varepsilon}_0^p \Big[\frac{y_{eq}}{(1+\theta^p)\sigma_0^p}\Big]^m \frac{\mathbf{s}-\mathbf{a}}{y_{eq}} \qquad \dot{\boldsymbol{\varepsilon}}^c = \frac{3}{2}\dot{\varepsilon}_0^c \Big[\frac{\sigma_{eq}}{(1+\theta^c)\sigma_0^c}\Big]^n \frac{\mathbf{s}}{\sigma_{eq}} \tag{3.2}$$

where $\boldsymbol{\sigma}$ is the stress, $\mathbf{D}^e$ is the isotropic elastic stiffness, $\dot{\varepsilon}_0^p$, σ_0^p, and m are viscoplastic parameters, $\mathbf{s}$ is the deviatoric stress, $\mathbf{a}$ is the deviatoric back stress, $\dot{\varepsilon}_0^c$, σ_0^c, and n are creep parameters, θ^p and θ^c are variables representing the effects of cyclic hardening on $\dot{\boldsymbol{\varepsilon}}^p$ and $\dot{\boldsymbol{\varepsilon}}^c$, respectively, and y_{eq} and σ_{eq} are defined as

$$y_{eq} = \sqrt{\frac{3}{2}}\|\mathbf{s}-\mathbf{a}\| \qquad \sigma_{eq} = \sqrt{\frac{3}{2}}\|\mathbf{s}\| \tag{3.3}$$

It is further assumed that the back stress can be decomposed into M parts (Chaboche *et al.*, 1979; Chaboche, 2008)[2], and that cyclic hardening equally affects the drag and back stresses (Ohno *et al.*, 1998, 2017a)[3]. In addition, it is assumed that the evolution of each part of the back stress is represented by the Ohno-Wang model (Ohno and Wang, 1993). We thus use the following equations for $\mathbf{a}$

$$\begin{aligned} &\mathbf{a} = (1+\theta^p)\widetilde{\mathbf{a}} \qquad \widetilde{\mathbf{a}} = \sum_{i=1}^{M} h^{(i)}\mathbf{b}^{(i)} \\ &\dot{\mathbf{b}}^{(i)} = \frac{2}{3}\dot{\boldsymbol{\varepsilon}}^p - \zeta^{(i)}(\zeta^{(i)} b_{eq}^{(i)})^{k^{(i)}} \Big\langle \dot{\boldsymbol{\varepsilon}}^p : \frac{\mathbf{b}^{(i)}}{b_{eq}^{(i)}} \Big\rangle \mathbf{b}^{(i)} \end{aligned} \tag{3.4}$$

where $\widetilde{\mathbf{a}}$ is the deviatoric back stress free of the effect of cyclic hardening, $\mathbf{b}^{(i)}$ is the i-th non-dimensional back stress related to $\widetilde{\mathbf{a}}$, $h^{(i)}$ is the i-th incipient kinematic hardening modulus, $\zeta^{(i)}$ and $k^{(i)}$ are parameters of the back stress evolution, and $b_{eq}^{(i)}$ is defined as

$$b_{eq}^{(i)} = \sqrt{\frac{3}{2}}\|\mathbf{b}^{(i)}\| \tag{3.5}$$

Austenitic stainless steels exhibit a marked dependence of cyclic hardening on the strain range (e.g., Chaboche *et al.*, 1979; Ohno, 1982; Kang *et al.*, 2003). Hence, we assume the following equation for θ^p in Eqs. $(3.2)_1$ and $(3.4)_1$

$$\theta^p = \phi(\Delta\varepsilon^p)\kappa \tag{3.6}$$

where $\phi(\Delta\varepsilon^p)$ is the material function representing the dependence of cyclic hardening on the viscoplastic strain range $\Delta\varepsilon^p$, and κ is the cyclic hardening parameter, which evolves as

$$\dot{\kappa} = L(\kappa_0 - \kappa)\dot{p} - R\kappa^{\omega} \tag{3.7}$$

Here, L and κ_0 are strain hardening parameters, R and ω are thermal recovery parameters, and $\dot{p}$ denotes the accumulating rate of viscoplastic strain

$$\dot{p} = \sqrt{\frac{2}{3}}\|\dot{\boldsymbol{\varepsilon}}^p\| \tag{3.8}$$

[1]Eqs. (3.1)-(3.3) based on the decomposition of the inelastic strain-rate into viscoplastic and creep components were assumed for solders in the absence of cyclic hardening (Kobayashi *et al.*, 2003).

[2]The multiple back stresses can be transformed to the multiple surfaces proposed by Mróz (1967), as shown by Ohno and Wang (1991).

[3]Trampczynski (1988) experimentally showed the effect of cyclic hardening on the back stress using the technique of successive unloading.

Equation (3.7) does not represent the cyclic softening following cyclic hardening that was observed in the creep-fatigue tests (Fig. 3). However, this limitation is allowed for the purpose of simulating the cyclic hardening and stress relaxation behavior discussed in Section 2.2.

The creep strain-rate $\dot{\boldsymbol{\varepsilon}}^c$ may be affected by cyclic hardening because grain boundary sliding can be accommodated with dislocation viscoplasticity as demonstrated by Crossman and Ashby (1975). This effect is represented by θ^c in Eq. $(3.2)_2$. We assume

$$\theta^c = c\theta^p \tag{3.9}$$

where c is a parameter representing the effect of cyclic hardening on $\dot{\boldsymbol{\varepsilon}}^c$.

The constitutive model described in this Section needs $\Delta\varepsilon^p$ to be evaluated during computation. We can use the resetting scheme of a viscoplastic strain surface to correctly evaluate $\Delta\varepsilon^p$ (Ohno *et al.*, 2017b). This plastic-strain-range (PSR) surface has the same expression as the memory surface of Chaboche *et al.* (1979), and follows the same evolution rule as that of Ohno (1982). In the resetting scheme, however, the PSR surface is reset to a point and re-evolves every cycle under cyclic loading. The resetting thus provides a definite value for the evolution parameter η of the PSR surface irrespective of the amount of cyclic hardening, pre-straining, and ratcheting. In this study, η is set to 0.4, as verified by Ohno *et al.* (2017b).

4. Determination of material parameters

Table 4 gives the material parameters used in this study, which were determined using the following procedure. In the table, E and ν denote Young's modulus and Poisson's ratio, respectively.

Table 4. Material parameters with stress in MPa, strain in mm/mm, and time in s

Elastic	$E = 1.44 \cdot 10^5$, $\nu = 0.30$
Viscoplastic	$\dot{\varepsilon}_0^p = 10^{-3}$, $\sigma_0^p = 7.53 \cdot 10^1$, $m = 20.0$
Creep	$\dot{\varepsilon}_0^c = 10^{-3}$, $\sigma_0^c = 2.72 \cdot 10^2$, $n = 10.9$
Kinematic hardening	$h^{(1)} = 1.63 \cdot 10^5$, $h^{(2)} = 3.81 \cdot 10^4$, $h^{(3)} = 9.27 \cdot 10^3$, $h^{(4)} = 1.59 \cdot 10^3$, $h^{(5)} = 7.24 \cdot 10^2$
	$\zeta^{(1)} = 6.67 \cdot 10^3$, $\zeta^{(2)} = 2.00 \cdot 10^3$, $\zeta^{(3)} = 6.67 \cdot 10^2$, $\zeta^{(4)} = 2.50 \cdot 10^2$, $\zeta^{(5)} = 1.25 \cdot 10^2$
	$k^{(i)} = 3.0$, $(i = 1, 2, \ldots, 5)$
Cyclic hardening	$\kappa_0 = 0.726$, $L = 13.4$, $R = 0.411$, $\omega = 13.6$, $c = 0.32$
	$\lambda = 4.00 \cdot 10^2$, $\Delta\varepsilon_0^p = 6.61 \cdot 10^{-3}$
PSR surface evolution	$\eta = 0.40$

1. The initial tensile curve at $\dot{\varepsilon} = 10^{-3}\,\mathrm{s}^{-1}$ was fitted, as shown in Fig. 4. This fitting was made using in-house developed Excel software assuming that cyclic hardening and creep strain-rate were negligible under initial tensile loading. The initial tensile curve was on-line fitted by numerically integrating the constitutive equations in the Excel software. Among the parameters, $\dot{\varepsilon}_0^p$ was selected to be $\dot{\varepsilon}_0^p = 10^{-3}\,\mathrm{s}^{-1}$, and $k^{(i)}$, responsible for ratcheting, was set to 3.0 (Ohno *et al.*, 2016a). The viscoplasticity exponent m had almost no influence on $\dot{\boldsymbol{\varepsilon}}^p$ at $\dot{\varepsilon} = 10^{-3}\,\mathrm{s}^{-1}$ because we selected $\dot{\varepsilon}_0^p = 10^{-3}\,\mathrm{s}^{-1}$ in Eq. $(3.2)_1$. Thus, σ_0^p, M, $h^{(i)}$, and $\zeta^{(i)}$ were determined.

2. Variations in σ_{+peak} with N in the fatigue tests at $\dot{\varepsilon} = 10^{-3}\,\mathrm{s}^{-1}$ with $\Delta\boldsymbol{\varepsilon} = 0.01$, 0.007 and 0.004 were used to determine L, κ_0, and $\phi(\Delta\varepsilon^p)$. It is shown that the constitutive

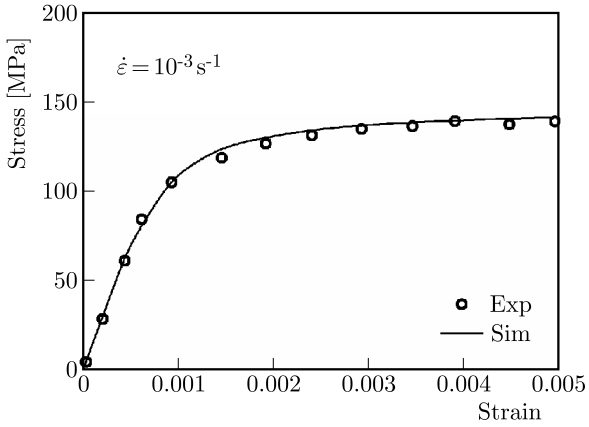

Fig. 4. Tensile stress-strain relationship at $\dot{\varepsilon} = 10^{-3}\,\mathrm{s}^{-1}$

model gives the following relationships to σ_{+peak} in the absence of thermal recovery of cyclic hardening (Appendix A)[4]

$$\frac{\sigma_{+peak} - \sigma^{ini}_{+peak}}{\sigma^{sat}_{+peak} - \sigma^{ini}_{+peak}} = 1 - \exp(-Lp) \qquad \frac{\sigma^{sat}_{+peak} - \sigma^{ini}_{+peak}}{\sigma^{ini}_{+peak}} = \phi(\Delta\boldsymbol{\varepsilon}^p)\kappa_0 \tag{4.1}$$

where σ^{ini}_{+peak} and σ^{sat}_{+peak} indicate the initial and saturated values of σ_{+peak}. Equations (4.1) were used to determine L, κ_0, and $\phi(\Delta\boldsymbol{\varepsilon}^p)$ (Figs. 5a and 5b). The following form of $\phi(\Delta\boldsymbol{\varepsilon}^p)$ was found appropriate in the present study

$$\phi(\Delta\varepsilon^p) = \frac{1 - \exp(-\lambda\Delta\varepsilon^p)}{1 - \exp(-\lambda\Delta\varepsilon^p_0)} \tag{4.2}$$

where λ is a fitting parameter, and $\Delta\varepsilon^p_0$ is selected to be equal to the saturated viscoplastic strain range in the fatigue test at $\dot{\varepsilon} = 10^{-3}\,\mathrm{s}^{-1}$ and $\Delta\varepsilon = 0.01$.

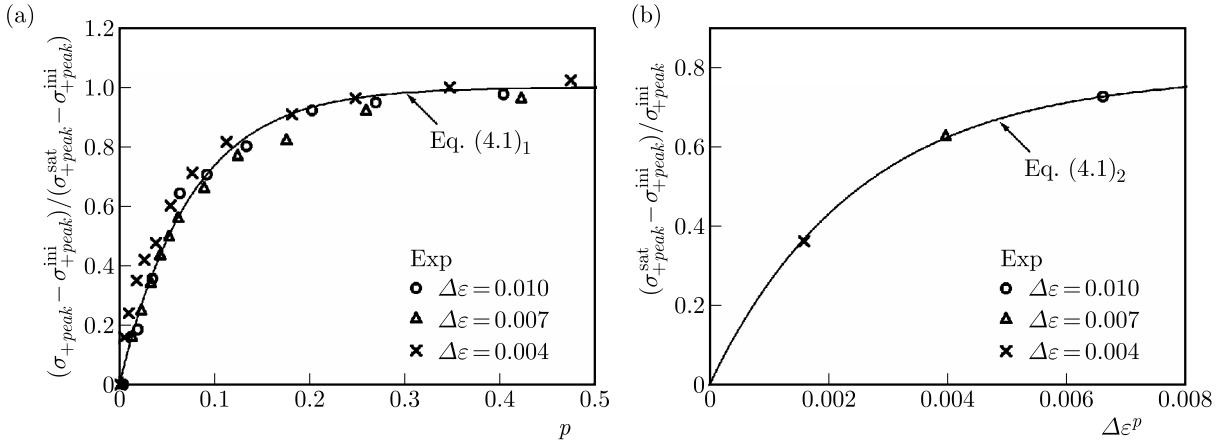

Fig. 5. (a) Change in σ_{+peak} with the accumulated viscoplastic strain p and (b) dependence of saturated σ_{+peak} on the viscoplastic strain range $\Delta\varepsilon^p$ in the fatigue tests at $\dot{\varepsilon} = 10^{-3}\,\mathrm{s}^{-1}$

3. The thermal recovery parameters R and ω in Eq. (3.7) were determined to represent the effect of strain hold time t_h on σ_{+peak} at $N \approx 20$ in the creep-fatigue tests at $\dot{\varepsilon} = 10^{-3}\,\mathrm{s}^{-1}$ with $t_h = 10\,\mathrm{min}$ and $60\,\mathrm{min}$ at $\Delta\varepsilon = 0.01$ (Appendix B).

[4]Goodall *et al.* (1981) first showed Eq. $(4.1)_1$ for fitting the tensile peak stress data of 316 stainless steel at 600°C.

4. The Norton-stage data under strain holding at $N = 1$ and 20 in the creep-fatigue test at $\dot{\varepsilon} = 10^{-3}\,\mathrm{s}^{-1}$ with $t_h = 60\,\mathrm{min}$ at $\Delta\varepsilon = 0.01$ were fitted, as shown by the solid and dashed lines in Fig. 2a. The fitting at $N = 1$ was used to determine σ_0^c and n in Eq. $(3.2)_2$ by selecting $\dot{\varepsilon}_0^c = 10^{-3}\,\mathrm{s}^{-1}$ with negligible cyclic hardening, $\theta^c \simeq 0$, at $N = 1$. The fitting at $N = 20$ was then used to estimate c in Eq. (3.9) to reproduce the small increase in $\sigma_{10\mathrm{E}-7}$ depicted in Fig. 3 (Appendix C)

$$c \simeq \frac{\sigma_{10\mathrm{E}-7}^{N=20}/\sigma_{10\mathrm{E}-7}^{ini} - 1}{\sigma_{+peak}^{N=20}/\sigma_{+peak}^{ini} - 1} \tag{4.3}$$

where $\sigma_{10\mathrm{E}-7}^{N=20}$ and $\sigma_{+peak}^{N=20}$ denote the values of $\sigma_{10\mathrm{E}-7}$ and σ_{+peak} at $N = 20$, respectively.

5. The saturated hysteresis loops in the fatigue tests at $\dot{\varepsilon} = 10^{-3}\,\mathrm{s}^{-1}$ and $10^{-4}\,\mathrm{s}^{-1}$ at $\Delta\varepsilon = 0.01$ were fitted to determine the viscoplasticity exponent m (Fig. 6).

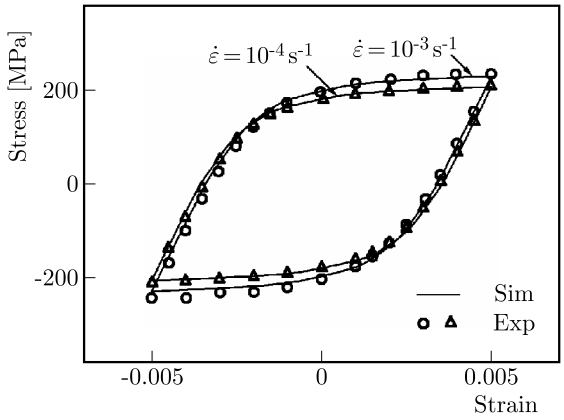

Fig. 6. Saturated stress-strain hysteresis loops in the fatigue tests at $\dot{\varepsilon} = 10^{-3}\,\mathrm{s}^{-1}$ and $10^{-4}\,\mathrm{s}^{-1}$ at $\Delta\varepsilon = 0.01$

5. Comparison of simulated and experimental results

The creep-fatigue tests were simulated using the constitutive model described in Section 3 with the material parameters given in Table 4. The constitutive model was implemented in Abaqus using a user subroutine UMAT by extending the UMAT program developed by Ohno *et al.* (2016b, 2017b). From here on, t^* denotes the time elapsed after the onset of strain holding, and σ_{relax} indicates the stress attained at the end of stress relaxation under strain holding. It is restated that the cyclic softening following cyclic hardening is disregarded in the constitutive model. This limitation is allowed in simulating the transient and Norton stages affected differently by cyclic hardening. Accordingly, this Section compares the simulated and experimental results with emphasis on the stress relaxation behavior under strain holding at cycles where cyclic softening was not significant.

The tensile peak stress variations and stress relaxation curves observed in the creep-fatigue tests at $\dot{\varepsilon} = 10^{-3}\,\mathrm{s}^{-1}$ with $t_h = 60\,\mathrm{min}$ at $\Delta\varepsilon = 0.007$ and 0.01 were simulated with good accuracy, as shown in Figs. 7 and 8. The variations in σ_{relax} with N in the two tests were also simulated well, though σ_{relax} was slightly inaccurate in the case of $\Delta\varepsilon = 0.007$ (Fig. 7). The stress relaxation became more significant as cyclic hardening developed in both the experimental and simulated results. Ignoring $\dot{\boldsymbol{\varepsilon}}^c$ in the constitutive model did not affect the transient stage under strain holding, but resulted in considerably under-predicting the stress relaxation, as shown in Figs. 9a and 9b in the case of $\Delta\varepsilon = 0.01$ with $t_h = 60\,\mathrm{min}$. Hence, accurate simulation of the

stress relaxation shown in Figs. 7 and 8 was owing to the dominance of $\dot{\varepsilon}^p$ and $\dot{\varepsilon}^c$ in the transient and Norton stages, respectively. Therefore, the addition of $\dot{\varepsilon}^c$ to $\dot{\varepsilon}^p$ and the Norton type of creep equation expressed as Eq. $(3.2)_2$ for $\dot{\varepsilon}^c$ enabled accurate simulation of the stress relaxation under strain holding.

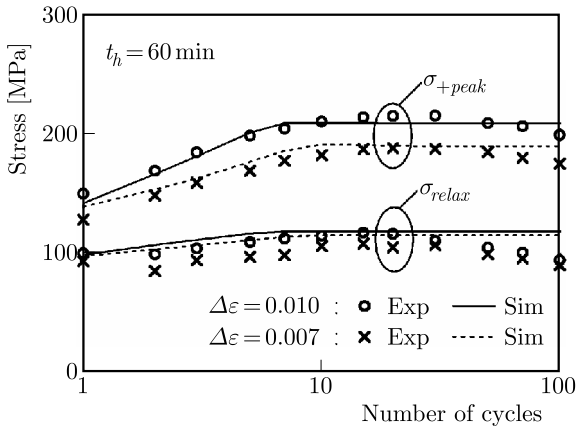

Fig. 7. Variations in σ_{+peak} and σ_{relax} with N and $\Delta\varepsilon$ under creep-fatigue loading at $\dot{\varepsilon} = 10^{-3}\,\mathrm{s}^{-1}$ with $t_h = 60$ min

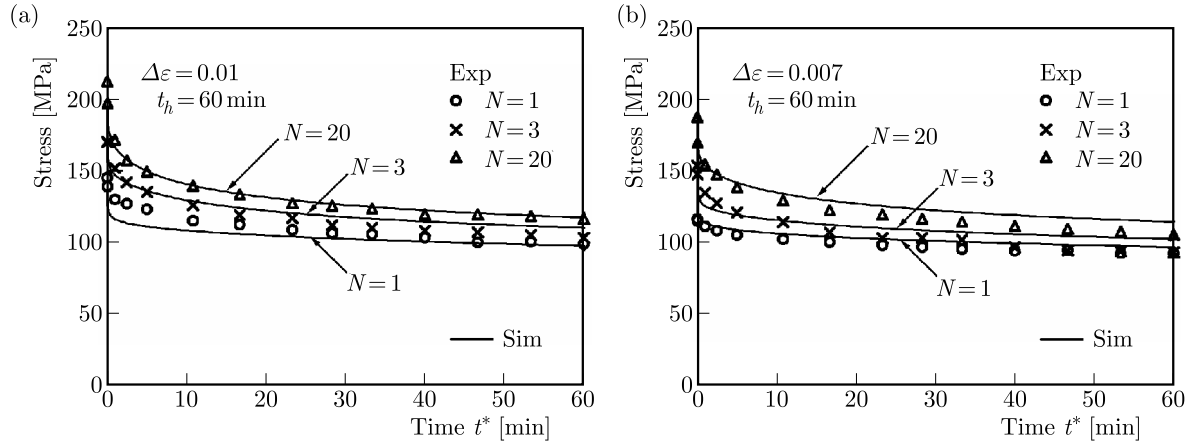

Fig. 8. Stress relaxation under creep-fatigue loading at $\dot{\varepsilon} = 10^{-3}\,\mathrm{s}^{-1}$ with $t_h = 60$ min at: (a) $\Delta\varepsilon = 0.01$ and (b) $\Delta\varepsilon = 0.007$

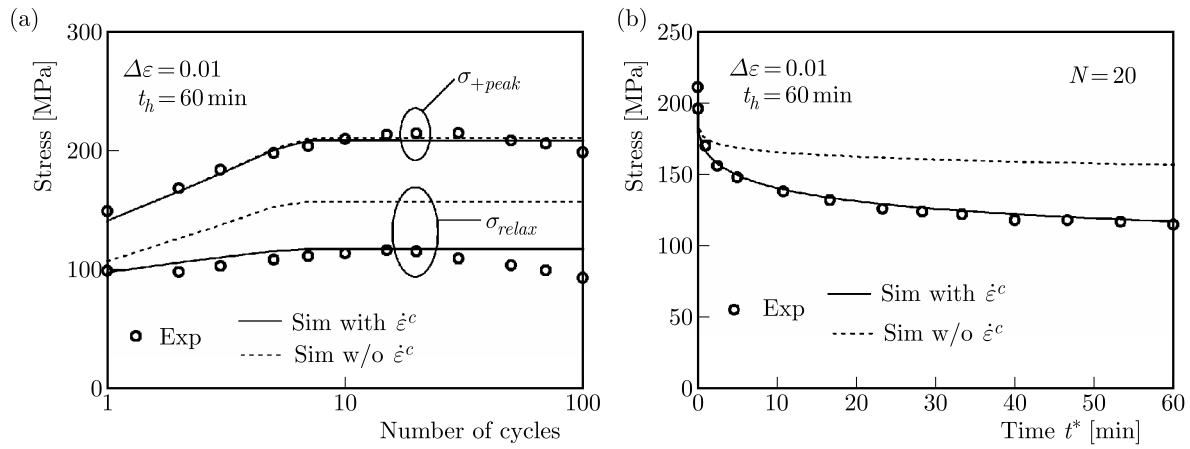

Fig. 9. Effect of the creep strain-rate on (a) variations in σ_{+peak} and σ_{relax} with N and (b) stress relaxation at $N = 20$ under creep-fatigue loading at $\dot{\varepsilon} = 10^{-3}\,\mathrm{s}^{-1}$ with $t_h = 60$ min at $\Delta\varepsilon = 0.01$

The effect of cyclic hardening on $\dot{\varepsilon}^c$ was taken into account through θ^c in Eq. $(3.2)_2$ in the constitutive model, and θ^c was assumed to be proportional to θ^p, $\theta^c = c\theta^p$, in Eq. (3.9). Figure 10 demonstrates the effect of c on the stress relaxation in the simulation of the creep--fatigue test at $\dot{\varepsilon} = 10^{-3}\,\mathrm{s}^{-1}$ with $t_h = 60\,\mathrm{min}$ at $\Delta\varepsilon = 0.01$. As shown in Fig. 10b, the stress relaxation at $N = 20$ was slightly over-predicted if $c = 0$, whereas it was noticeably under--predicted if $c = 1$. If $c = 0$ cyclic hardening had no effect on $\dot{\varepsilon}^c$ through θ^c, and if $c = 1$ cyclic hardening had the same effect on $\dot{\varepsilon}^c$ and $\dot{\varepsilon}^p$. Selecting $c = 0.32$ (i.e., $\theta^c \approx \theta^p/3$) was found to be appropriate for simulating the stress relaxation. It was thus shown that $\dot{\varepsilon}^c$ was much less affected by cyclic hardening than $\dot{\varepsilon}^p$, leading to suggestion that inelastic deformation mechanisms different from viscoplasticity started to operate shortly after the onset of strain holding, as discussed in Section 2.

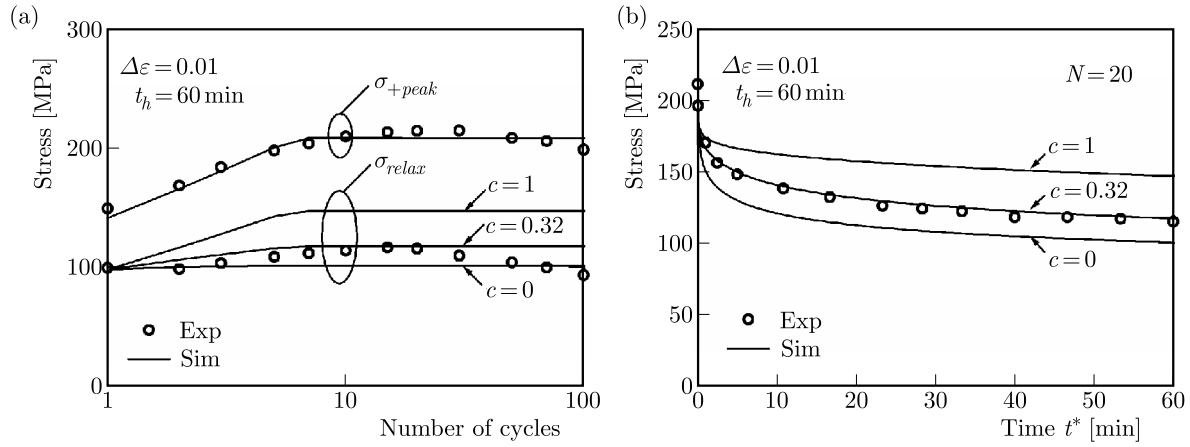

Fig. 10. Effect of the cyclic hardening parameter c on (a) variations in σ_{+peak} and σ_{relax} with N and (b) stress relaxation at $N = 20$ under creep-fatigue loading at $\dot{\varepsilon} = 10^{-3}\,\mathrm{s}^{-1}$ with $t_h = 60\,\mathrm{min}$ at $\Delta\varepsilon = 0.01$

Figure 11 illustrates the effects of t_h on σ_{+peak} and σ_{relax} measured in the creep-fatigue tests at $\dot{\varepsilon} = 10^{-3}\,\mathrm{s}^{-1}$ with $t_h = 10\,\mathrm{min}$ and $60\,\mathrm{min}$ at $\Delta\varepsilon = 0.01$. In Fig. 11a, σ_{+peak} for $t_h = 0$ is shown for reference. In the two tests with $t_h = 10$ and $60\,\mathrm{min}$, the effect of t_h on σ_{+peak} appeared slightly after the near-saturation of cyclic hardening, whereas the effect on σ_{relax} became rather large with increasing N before the near-saturation of cyclic hardening. These experimental features were well reproduced by the constitutive model. The creep-fatigue tests at $\Delta\varepsilon = 0.007$ with $t_h = 10$ and $60\,\mathrm{min}$ were also simulated accurately, though not shown here to save the space.

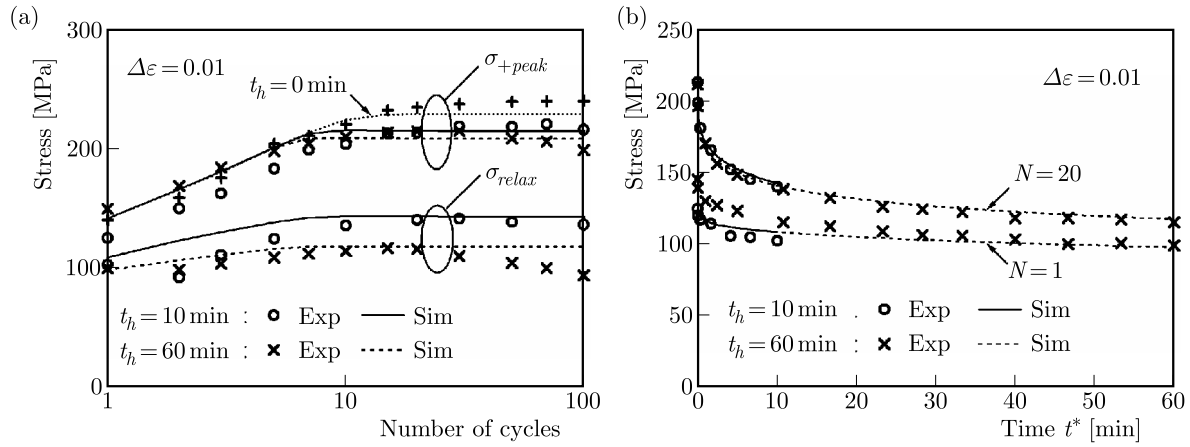

Fig. 11. Effect of the strain hold time t_h on (a) variations in σ_{+peak} and σ_{relax} with N and (b) stress relaxation at $N = 1$ and 20 under creep-fatigue loading at $\dot{\varepsilon} = 10^{-3}\,\mathrm{s}^{-1}$ at $\Delta\varepsilon = 0.01$

The slight effect of t_h on σ_{+peak} described above was successfully simulated because of the thermal recovery of cyclic hardening represented by the second term on the right-hand side of Eq. (3.7). Here, it is noted that the thermal recovery exponent ω in Eq. (3.7) is large (Table 4); as a result, the thermal recovery of cyclic hardening occurred non-linearly to yield the slight effect of t_h on σ_{+peak} despite the factor of six difference in t_h in the two tests with $t_h = 10$ and 60 min. However, the comparatively large effect of t_h on σ_{relax} was well simulated owing to $\dot{\varepsilon}^c$ expressed as Eq. $(3.2)_2$, as depicted in Fig. 11b. Because σ_{relax} denotes the stress attained at the end of stress relaxation, it is seen from Fig. 11b that the difference in σ_{relax} in the two tests was caused by the stress relaxation during $10 \leqslant t^* \leqslant 60$ min in the test with $t_h = 60$ min; the stress relaxation from $t^* = 10$ min to $t^* = 60$ min was about 10 MPa and 25 MPa at $N = 1$ and 20, respectively. The stress relaxation during $10 \leqslant t^* \leqslant 60$ min was in the Norton stage. Therefore, the difference in σ_{relax} in the two tests was well simulated because of the Norton type of creep equation expressed as Eq. $(3.2)_2$ for $\dot{\varepsilon}^c$.

The stress relaxation under strain holding became larger with the development of cyclic hardening or with the increase in the strain hold time, as shown in this Section. Goodall *et al.* (1981) observed this feature in creep-fatigue tests of 316 stainless steel at 600°C, and Nouailhas (1989) simulated the tests using a unified model of cyclic viscoplasticity. However, Goodall *et al.* (1981) and Nouailhas (1989) did not notice the transient and Norton stages in stress relaxation, which were studied in this work; moreover, Nouailhas (1989) did not show stress relaxation curves under strain holding.

6. Concluding remarks

In this work, the cyclic hardening and stress relaxation behavior of SUS316HTP was experimentally and numerically studied under cyclic loading with tensile strain holding at 700°C. Creep-fatigue tests were performed to show that the slow stress-relaxation stage satisfying Norton's law followed the transient stress-relaxation stage under strain holding. The Norton stage was much less affected by cyclic hardening than the transient stage. Since the transient stage was rate-controlled by viscoplasticity in the presence of the increase in dislocation density in grains to cause cyclic hardening, it was suggested that inelastic deformation mechanisms, such as diffusion creep and grain boundary sliding, operated in the Norton stage.

A cyclic viscoplastic-creep model was developed based on the experimental results described above. In this model, the inelastic strain-rate $\dot{\varepsilon}^{in}$ was decomposed into viscoplastic and creep strain-rates, which were dominant in the transient and Norton stages in stress relaxation, respectively. The viscoplastic strain-rate $\dot{\varepsilon}^p$ was expressed by incorporating the noticeable effect of cyclic hardening on the drag and back stresses, while the creep strain-rate $\dot{\varepsilon}^c$ was ruled by Norton's law and was assumed to be weakly affected by cyclic hardening. The material parameters in the constitutive model were determined to verify the decomposition of $\dot{\varepsilon}^{in}$ into $\dot{\varepsilon}^p$ and $\dot{\varepsilon}^c$, which were affected differently by cyclic hardening.

Finally, the cyclic viscoplastic-creep model was used to simulate the creep-fatigue tests performed in the present study. The constitutive model successfully simulated the stress relaxation behavior in the presence of cyclic hardening, and the stress relaxation in the simulation became more significant as cyclic hardening developed, as observed in the creep-fatigue tests. This was owing to the dominance of $\dot{\varepsilon}^p$ and $\dot{\varepsilon}^c$ in the transient and Norton stages, respectively, resulting in the transient stage being much more affected by cyclic hardening than the Norton stage. The stress-relaxation curves were also accurately simulated, and the effect of t_h on the stress relaxation was attributed to $\dot{\varepsilon}^c$ in the Norton stage.

Appendix A. Change in tensile peak stress

Let us consider rapid, uniaxial cyclic loading with $t_h = 0$ to ignore $\dot{\boldsymbol{\varepsilon}}^c$. On the tension side, Eqs. $(3.2)_1$, $(3.4)_1$ and (3.6) give the following equation in the viscoplastic region, where $\dot{\varepsilon}^p \simeq \dot{\varepsilon}$

$$\sigma \simeq (1+\phi\kappa)\Big[\sigma_0^p\Big(\frac{\dot{\varepsilon}}{\dot{\varepsilon}_0^p}\Big)^{1/m} + \widetilde{\alpha}\Big] \tag{A.1}$$

where $\widetilde{\alpha}$ indicates the uniaxial component of the cyclic-hardening-free back stress. Because cyclic hardening is negligibly small under the initial loading to the first tensile peak, Eq. (A.1) allows the initial tensile peak stress σ_{+peak}^{ini} to be expressed as

$$\sigma_{+peak}^{ini} \simeq \sigma_0^p\Big(\frac{\dot{\varepsilon}}{\dot{\varepsilon}_0^p}\Big)^{1/m} + \widetilde{\alpha}_{+peak}^{ini} \tag{A.2}$$

where $\widetilde{\alpha}_{+peak}^{ini}$ denotes the initial peak value of $\widetilde{\alpha}$. Here, let us assume that the tensile peak value $\widetilde{\alpha}_{+peak}$ does not change from $\widetilde{\alpha}_{+peak}^{ini}$ with the increasing N because $\widetilde{\alpha}$ is regarded as the back stress in the absence of cyclic hardening. Eqs. (A.1) and (A.2) thus provide

$$\sigma_{+peak} \simeq (1+\phi\kappa)\sigma_{+peak}^{ini} \tag{A.3}$$

When the thermal recovery of cyclic hardening is negligible under rapid cyclic loading, Eq. (3.7) is integrated to give

$$\kappa = \kappa_0[1-\exp(-Lp)] \tag{A.4}$$

Hence, Eq. (A.3) leads to Eqs. (4.1).

Appendix B. Determination of thermal recovery parameters

Let us consider rapid, uniaxial cyclic loading with $t_h \neq 0$ to determine the thermal recovery parameters R and ω in Eq. (3.7). Let us suppose that κ decreases from κ_{+peak} to κ_{relax} under tensile strain holding, and that κ increases from κ_{relax} to κ_{+peak} under rapid cyclic loading in one cycle. Here, we assume that the second and first terms on the right-hand side in Eq. (3.7) are active under tensile strain holding and rapid cyclic loading, respectively, to provide

$$\begin{aligned} \kappa_{relax} &= [\kappa_{+peak}^{1-\omega} + R(\omega-1)t_h]^{1/(1-\omega)} \\ \kappa_{+peak} &= \kappa_{relax} + (\kappa_0 - \kappa_{relax})[1-\exp(-Lp^*)] \end{aligned} \tag{B.1}$$

where p^* denotes the change in p due to rapid cyclic loading in one cycle

$$p^* = 2\Big(\Delta\varepsilon - \frac{\sigma_{relax} + |\sigma_{-peak}|}{E}\Big) \tag{B.2}$$

To determine R and ω using Eqs. (B.1), the tensile peak stresses at $N = 30$ in the creep-fatigue tests at $\dot{\varepsilon} = 10^{-3}\,\mathrm{s}^{-1}$ with $t_h = 10\,\mathrm{min}$ and $60\,\mathrm{min}$ at $\Delta\varepsilon = 0.01$ are used to evaluate $\kappa_{+peak10}$ and $\kappa_{+peak60}$ using Eq. (A.3) as

$$\kappa_{+peak10} = \frac{1}{\phi}\Big(\frac{\sigma_{+peak10}}{\sigma_{+peak}^{ini}} - 1\Big) \qquad \kappa_{+peak60} = \frac{1}{\phi}\Big(\frac{\sigma_{+peak60}}{\sigma_{+peak}^{ini}} - 1\Big) \tag{B.3}$$

where the subscripts 10 and 60 indicate $t_h = 10\,\mathrm{min}$ and $60\,\mathrm{min}$. Then, $\kappa_{relax10}$ and $\kappa_{relax60}$ are calculated using Eq. $(B.1)_2$. Here, it is noted that ϕ, κ_0, and L are determined in Step 2 in Section 4. Finally, R and ω are evaluated by numerically solving the following equations derived from Eq. $(B.1)_1$

$$\begin{aligned} \kappa_{relax10}^{1-\omega} - \kappa_{+peak10}^{1-\omega} &= R(\omega-1)t_{h10} \qquad & t_{h10} &= 600\,\mathrm{s} \\ \kappa_{relax60}^{1-\omega} - \kappa_{+peak60}^{1-\omega} &= R(\omega-1)t_{h60} \qquad & t_{h60} &= 3600\,\mathrm{s} \end{aligned} \tag{B.4}$$

Appendix C. Cyclic hardening parameter for creep strain-rate

To evaluate c in Eq. (3.9), we consider the changes in σ_{+peak} and $\sigma_{10\mathrm{E}-7}$ with N in the creep-fatigue test at $\dot{\varepsilon} = 10^{-3}\,\mathrm{s}^{-1}$ with $t_h = 60\,\mathrm{min}$ at $\Delta\varepsilon = 0.01$. For σ_{+peak} in this creep-fatigue test, Eq. (A.3) is valid, though κ is affected by $t_h \neq 0$. For $\sigma_{10\mathrm{E}-7}$, Eqs. $(3.2)_2$, (3.6) and (3.9) provide

$$\sigma_{10\mathrm{E}-7} = (1 + c\phi\kappa)\sigma^{ini}_{10\mathrm{E}-7} \qquad \sigma^{ini}_{10\mathrm{E}-7} = \sigma^c_0\Big(\frac{\dot{\varepsilon}^c}{\dot{\varepsilon}^c_0}\Big)^{1/n} \tag{C.1}$$

where $\dot{\varepsilon}^c = 10^{-7}\,\mathrm{s}^{-1}$. The change in κ is considered small under strain holding when ω is large in Eq. (3.7). Thus, using Eqs. (A.3) and $(\mathrm{C}.1)_1$, c is estimated as

$$c \simeq \frac{\sigma_{10\mathrm{E}-7}/\sigma^{ini}_{10\mathrm{E}-7} - 1}{\sigma_{+peak}/\sigma^{ini}_{+peak} - 1} \tag{C.2}$$

Acknowledgment

We thank Melissa Gibbons, PhD, from Edanz Group (www.edanzediting.com/ac) for editing a draft of this manuscript.

References

1. Ainsworth R.A., 2006, R5 procedures for assessing structural integrity of components under creep and creep-fatigue conditions, *International Materials Reviews*, **51**, 107-126
2. Chaboche J.L., 2008, A review of some plasticity and viscoplasticity constitutive theories, *International Journal of Plasticity*, **24**, 1642-1693
3. Chaboche J.L., Dang Van K., Cordier G., 1979, Modelization of the strain memory effect on the cyclic hardening of 316 stainless steel, *Proceedings of the 5th International Conference on Structural Mechanics in Reactor Technology*, **L**, L11/3
4. Crossman F.W., Ashby M.F., 1975, The non-uniform flow of polycrystals by grain-boundary sliding accommodated by power-law creep, *Acta Metallurgica*, **23**, 425-440
5. Goodall I.W., Hales R., Walters D.J., 1981, On constitutive relations and failure criteria of an austenitic steel under cyclic loading at elevated temperature, *Creep in Structures*, Springer-Verlag, 103-127
6. Hales R., 1980, A quantitative metallographic assessment of structural degradation of type 316 stainless steel during creep-fatigue, *Fatigue of Engineering Materials and Structures*, **3**, 339-356
7. Hales R., 1983, A method of creep damage summation based on accumulated strain for the assessment of creep-fatigue endurance, *Fatigue of Engineering Materials and Structures*, **6**, 121-135
8. Inoue T., Igari T., Okazaki M., Sakane M., Tokimasa K., 1989, Fatigue-creep life prediction of 2.25Cr-1Mo steel by inelastic analysis, *Nuclear Engineering and Design*, **114**, 311-321
9. Kang G., Ohno N., Nebu A., 2003, Constitutive modeling of strain range dependent cyclic hardening, *International Journal of Plasticity*, **19**, 1801-1819
10. Kobayashi M., Mukai M., Takahashi H., Ohno N., Kawakami T., Ishikawa T., 2003, Implicit integration and consistent tangent modulus of a time-dependent non-unified constitutive model, *International Journal for Numerical Methods in Engineering*, **58**, 1523-1543
11. Krausz A.S., Krausz K., 1996, *Unified Constitutive Laws of Plastic Deformation*, Academic Press, San Diego

12. Miller A., 1976, An inelastic constitutive model for monotonic, cyclic, and creep deformation: Part 1 – equations development and analytical procedures, *Journal of Engineering Materials and Technology*, **98**, 97-105

13. Mróz Z., 1967, On the description of anisotropic workhardening, *Journal of the Mechanics and Physics of Solids*, **15**, 163-175

14. Nam S.W., 2002, Assessment of damage and life prediction of austenitic stainless steel under high temperature creep-fatigue interaction condition, *Materials Science and Engineering A*, **322**, 64-72

15. Nouailhas D., 1989, Unified modelling of cyclic viscoplasticity: Application to austenitic stainless steels, *International Journal of Plasticity*, **5**, 501-520

16. Ohno N., 1982, A constitutive model of cyclic plasticity with a nonhardening strain region, *Journal of Applied Mechanics*, **49**, 721-727

17. Ohno N., Abdel-Karim M., Kobayashi M., Igari T., 1998, Ratchetting characteristics of 316FR steel at high temperature, Part I: strain-controlled ratchetting experiments and simulations, *International Journal of Plasticity*, **14**, 355-372

18. Ohno N., Mizushima S., Okumura D., Tanie H., 2016a, Warpage variation analysis of Si/solder/Cu layered plates subjected to cyclic thermal loading, *Advanced Methods of Continuum Mechanics for Materials and Structures, Advanced Structured Materials*, **60**, 185-204

19. Ohno N., Tsuda M., Sugiyama H., Okumura D., 2016b, Elastic-viscoplastic implicit integration algorithm applicable to both plane stress and three-dimensional stress states, *Finite Elements in Analysis and Design*, **109**, 54-64

20. Ohno N., Wang J.D., 1991, Transformation of a nonlinear kinematic hardening rule to a multisurface form under isothermal and nonisothermal conditions, *International Journal of Plasticity*, **7**, 879-891

21. Ohno N., Wang J.D., 1993, Kinematic hardening rules with critical state of dynamic recovery, Part I: formulation and basic features for ratchetting behavior, *International Journal of Plasticity*, **9**, 375-390

22. Ohno N., Yamamoto R., Okumura D., 2017a, Thermo-mechanical cyclic hardening behavior of 304 stainless steel at large temperature ranges: Experiments and simulations, *International Journal of Mechanical Sciences* (article in press)

23. Ohno N., Yamamoto R., Sasaki T., Okumura D., 2017b, Resetting scheme for plastic strain surface in constitutive modeling of cyclic plasticity, *ZAMM – Zeitschrift für Angewandte Mathematik und Mechanik* (article in press, DOI: 10.1002/zamm.201700298)

24. Priest R.H., Ellison E.G., 1981, A combined deformation map-ductility exhaustion approach to creep-fatigue analysis, *Materials Science and Engineering*, **49**, 7-17

25. Takahashi Y., 1998, Evaluation of creep-fatigue life prediction methods for low-carbon nitrogen-added 316 stainless steel, *Journal of Engineering Materials and Technology*, **120**, 119-125

26. Takahashi Y., Shibamoto H., Inoue K., 2008, Study on creep-fatigue life prediction methods for low-carbon nitrogen-controlled 316 stainless steel (316FR), *Nuclear Engineering and Design*, **238**, 322-335

27. Trampczynski W., 1988, The experimental verification of the evolution of kinematic and isotropic hardening in cyclic plasticity, *Journal of the Mechanics and Physics of Solids*, **36**, 417-441

28. Yan X.L., Zhang X.C., Tu S.T., Mannan S.L., Xuan F.Z., Lin Y.C., 2015, Review of creep-fatigue endurance and life prediction of 316 stainless steels, *International Journal of Pressure Vessels and Piping*, **126-127**, 17-28

Manuscript received December 28, 2017; accepted for print March 1, 2018